KSCE Journal of Civil Engineering (2015) 19(6):1707-1715

DOI 10.1007/s12205-014-0685-x

Highway Engineering

pISSN 1226-7988, eISSN 1976-3808
www.springer.com/12205

Freeze Depth Predicting of Permafrost Subgrade based on Moisture and Thermal Coupling Model

Min Ye*, YanfangHufangfu, and Xuesong Mao*****

Received November 14, 2013/Revised May 26, 2014/Accepted September 2, 2014/Published Online December 12, 2014

Abstract

Water and heat conditions and the interactions between them are the key factors in highway freeze damage. A 2-D moisture-thermal coupling model has been developed to analyze the temperature profile of the permafrost subgrade and to more thoroughly understand the moisture and thermal transport in subgrade soil. The model accounts for the effects of heat generation, internal conduction and convection, and moisture transport to accurately predict the freeze depth of the subgrade. This model formulates the control equation of the temperature field, the moisture field and their coupling. A commercially available finite element package (ANSYS) is used to solve the simulation. The numerical calculations are compared with in-situ test results on the Qinghai-Tibet Highway and appear to be in strong agreement. The accuracy and precision of the coupling model are superior to the traditional single-field model, which indicates the model's suitability for predicting the freeze depth of the permafrost subgrade. This model can aid in prevention of highway damage by predicting periods of subgrade thaw and elevated water content such that traffic restrictions can be effectively implemented.

Keywords: *temperature field, moisture field, highway engineering, finite element method, freeze depth*

1. Introduction

The Qinghai-Tibet plateau is the youngest medium-low latitude plateau with an average altitude of more than 4000 m. The permafrost within the plateau covers approximately 147 km^2 and accounts for 60% of the entire permafrost area in China (Xu *et al.*, 2001). The Qinghai-Tibet Highway (QTH) runs for 632 km from north to south across the permafrost. Differential damages have occurred along the subgrade of the QTH over the past few years. The main damage types include cracking fracturing, pavement stepping, failed joints and pavement pumping, as shown in Fig. 1. The groundwater, the surface water and their freeze-thaw cycles are important factors affecting the dynamic characteristics of the subgrade soil, further induce the damages. The rising of groundwater and the infiltration of surface water will increase the internal water content of the highway, leading to non-uniform deformation. When the soil temperature is below 0ºC, the moisture transforms to the ice stage and the soil expands, resulting in cracking of the pavement surface. When the temperature rises, the ice in the subgrade begins to thaw. The thawing of the ice takes place from the pavement surface to the bottom of the subgrade. The bottom of the subgrade remains frozen, while the top of the subgrade has thawed. As a result, the moisture in the subgrade cannot infiltrate down. Therefore the pavement damage takes place. Soil freeze and thaw processes and the soil moisture distribution play critical roles in the hydrology and microclimate of frozen soil. Accurate simulations of the depth and time of freeze and the distribution of the soil water content provide important information to highway planning and freeze damage prevention.

The freeze and thaw cycle of the permafrost subgrade involves heat exchange, moisture migration and phase change. Traditionally, researchers have focused on the calculation and analysis of a single temperature field. In the 1960's, Russian scientists presented a moisture-thermal transmission model to study the soil freeze process. This model combined the one-dimensional thermal transfer equation and the one-dimensional seepage flow equation (Miller, 1972). Their model assumed that the moisture diffusion coefficient, the initial temperature and the water content of the soil are constant in the frosted and unfrosted soil. However, all of these coefficients vary over time. Thus, calculations based on this model cannot determine the real temperature profile of the soil. In the early 1970s R. L. Hanlan (Harlan, 1973) presented the Harlan model, which combined some new experiments and

*Associate Professor, National Engineering Laboratory for Highway Maintenance Equipment, Chang'an University, Xi'an 710064, China (Corresponding Author, E-mail: mingye@chd.edu.cn)

**M.Sc. Student, National Engineering Laboratory for Highway Maintenance Equipment, Chang'an University, Xi'an 710064, China (E-mail: 1107550844@qq.com)

***Professor, National Engineering Laboratory for Highway Maintenance Equipment, Chang'an University, Xi'an 710064, China (E-mail: xuesongmao@chd.edu.cn)

(a)

(b)

Fig. 1. Damage Pictures in the Field: (a) Cracking Damage, (b) Fracture Damage

observations. Harlan predicted that the power of the moisture migration in the soil depends on the water potential gradient. However, Harlan did not provide a method to determine the value of the water potential. Furthermore Taylor and Luthin models were developed to account for the thermal energy associated with moisture migration in the soil (Harlan and Nixon, 1979). However, these studies did not consider the heat exchange induced by moisture convection on the temperature field. With the rapid development of computer technology and the finite element method, commercially available programs have been extensively used in the scientific community in a wide variety of research since 2000. Examples of commercially available solutions for agricultural and geotechnical engineering include SVHeat (Soil Vision), Comsol and Ansys (Tekeste *et al.*, 2007; 2009; Xia, 2011; Wang *et al.*, 2010). Gatmiri, Behrouz derived the closed form two-dimensional fundamental solutions for a non-isothermal unsaturated deformable porous medium in both Laplace transform and time domains (Chen *et al.*, 2010). Klimenta, Dardan created a nonlinear Finite Element Method (FEM) model on the basis of an authentic case of fault caused by a previous mechanical damage of the cable sheath and insulation, as well as heat sources, thermo-physical and electrical material properties as functions of temperature and time S. (Fortino *et al.*, 2013). Fortino, Stefania proposed a FEM simulation of the hygro-thermal behaviour of wood under surface densification by using a three-dimensional hygro-thermal model based on earlier literature approaches (Gatmiri *et al.*, 2010). Trcala, Miroslav dealt with the numerical solution of a three-dimensional problem of non-isothermal moisture transfer in the anisotropic structure of wood and corresponding wood deformations in convective drying (Klimenta *et al.*, 2011). All these studies paves for the application of FEM method for the civil engineering. Chen *et al.* (2010) presented a new hybrid analytic-FEM approach for calculating coupling hygro-thermal deformation of concrete by using Matlab and ANSYS. However, these software tools are rarely applied to the highway engineering, for example, to couple several fields, which helps to illuminate the damage mechanisms present in the permafrost subgrade. This paper introduces an equation that couples the temperature and moisture fields of the subgrade by considering the thermal effects of moisture convection. This moisture-thermal coupling model is used to predict the soil temperature, freeze depth, and soil moisture of the QTH subgrade. The predictions of two models (single-field and coupled fields) are compared with the in-situ test results. This model can aid in prevention of highway damage by predicting periods of subgrade thaw and elevated water content such that traffic restrictions can be effectively implemented.

2. Natural Environment of QTH

2.1 Three Observation Sites Along QTH

The present QTH has a total length of 1937 km. 632 km of the QTH passes through the permafrost areas of the Qinghai-Tibetan Plateau, 550 km of which is in continuous permafrost zones and 82 km of which is in seasonal permafrost zones (Mao *et al.*, 2004), as shown in Fig. 2. In 1998, a research group at Chang'an University sets up three observation sites between Lhasa City and Golmud City along the highway to observe the ground temperature and rainfall in the subgrade. We have collected the infield data for more than ten years.

Two of the observation sites are located north of the Tanggula Mountains, one is in the Wudaoliang Mountain (K3006 + 100) and the other in the Tuotuo River (K3075 + 700). The third site is located south of the Tanggula Mountains in Anduo City (K3095

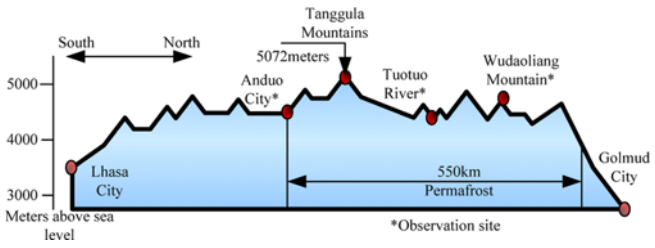

Fig. 2. Vertical Sectional Diagram (Golmud-Lhasa Section of QTH)

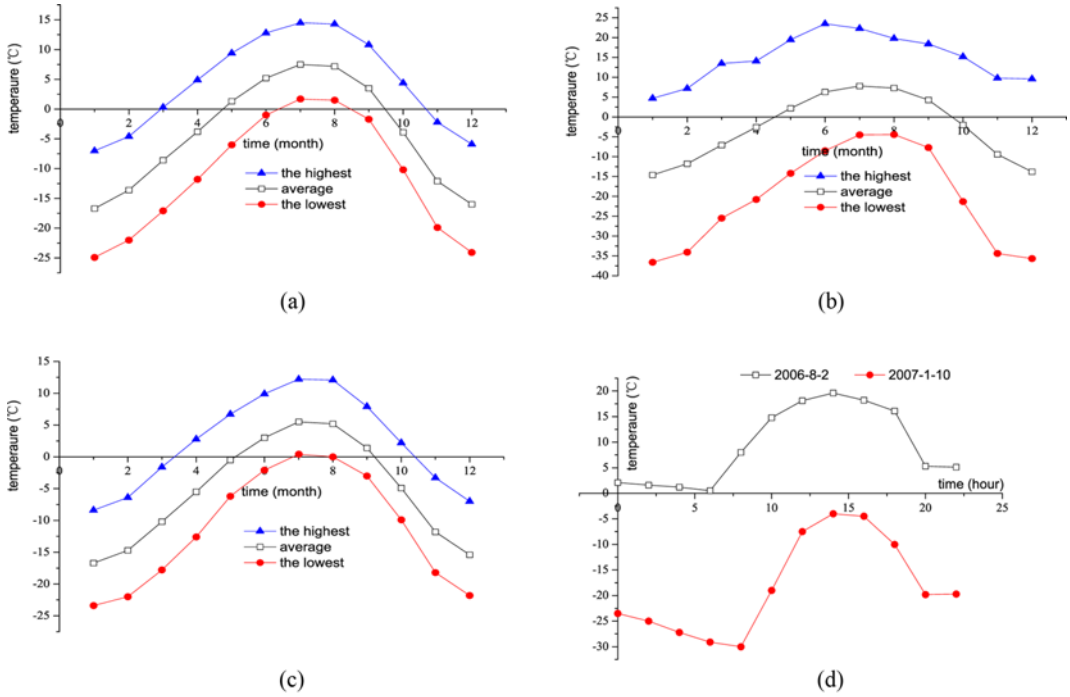

Fig. 3. Temperature Observation in QTH: (a) Annual Temperature at Wudaoliang Mountain, (b) Annual Temperature at Tuotuohe River, (c) Annual Temperature at Anduo City, (d) 24-hour Temperature Curve at Tuotuo River

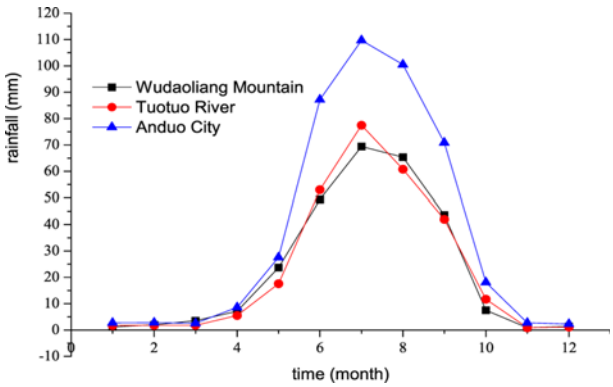

Fig. 4. Annual Rainfall for QTH

+ 600). The selection of these locations is based on their representation of the various types of permafrost in different ground temperature zones. The Wudaoliang Mountain, Tuotuo River and Anduo City represent low, middle and high temperature zones, respectively. The temperature and precipitation conditions of the three observation sites are presented in Figs. 3 and 4.

Figures 3(a), 3(b) and 3(c) show the ambient air temperatures at the three observation sites, where the annual average temperatures range from -2.1 to -6.2°C. The temperature decreases from the south (Anduo City) to the north (Wudaoliang Mountain) of the highway. The coldest month is January, and the hottest month is either July or August. The daily temperature at Tuotuo River (Fig. 3(d)), which is located along the middle portion of the highway, ranged from -3°C to -35°C on a winter day, the maximum temperature difference is approximately 30°C, and the coldest time is 6 AM. The daily temperature ranged from 0°C to 20°C on a summer day, the temperature difference is approximately 20°C, and the hottest time is 2 PM. The variation in the daily temperature at this site was very large. Therefore, the general characteristics of the climate along the QTH are that the annual average temperature is low and the daily temperature variation is high, particularly in the winter.

The annual rainfall curves presented in Fig. 4 show that rainfall is rare along the QTH and is primarily concentrated in the summer. The annual rainfalls at Tuotuo River and Wudaoliang Mountain (north of the Tanggula Mountains) range from 160 to 370 mm, and the rainfalls in July, August and September account for 90% of the annual rainfalls. The annual rainfall is 345 to 510 mm at Anduo City (south of the Tanggula Mountains), and the rainfall in July, August and September account for 65% of the annual rainfall. Rainfall is most likely to occur in the evening and is rare during the day. Evening rainfall makes up 50-60% of the total rainfall. Thunder showers and frozen precipitation are the main types of precipitation, while hail, sleet and snow can occur in any season.

2.2 *In-situ* Observation

Both the temperature and moisture data are acquainted from QTH in field. A 3-wire Resistance Temperature Detector (RTD) sensor PT100 is used for the temperature acquisition, as shown in Fig. 5(a). The temperature is acquainted by the self-developed equipment as shown in Fig. 5(c), whose core processor is a single chip processor ATmega16. The length of the PT100 sensor is 2 cm and protected by a steel tube. The wire length is varied from 2 m to 18 m, which is defined by the observation point. The

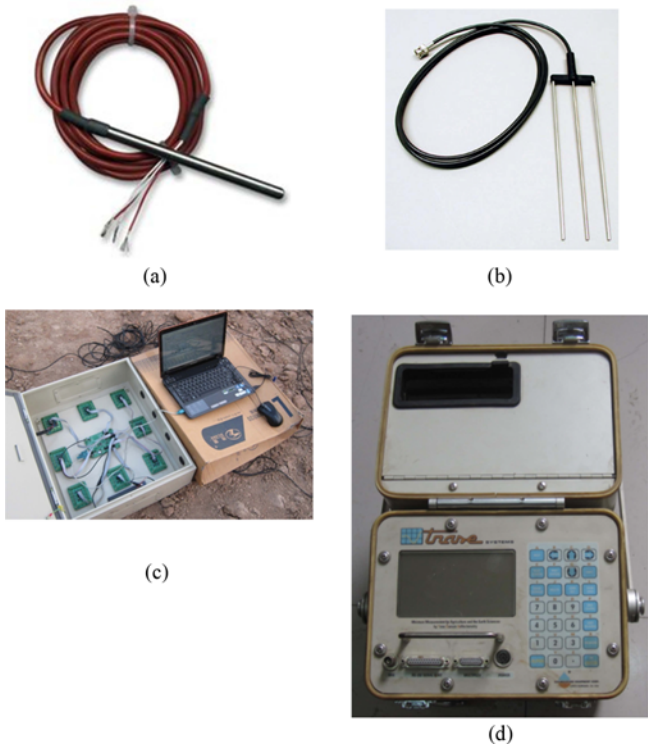

Fig. 5. Infield Data Acquisition Equipments: (a) Temperature Sensor, (b) Moisture Sensor, (c) Temperature Acquisition Equipment, (d) Moisture Acquisition Equipment

temperature acquisition accuracy is 0.01°C, which is enough for the highway engineering. A Time Domain Reflectometry (TDR) system is selected to acquaint the moisture of the subgrade. The moisture sensor is simple as shown in Fig. 5(b). The waveguide rods are 20 cm long and made of 0.3 cm diameter stainless steel rods. The moisture acquisition equipment is shown in Fig. 5(d), which is a TRASE System I, produced by the Soilmoisture Equipment Company. The TDR system is a self-contained, portable unit designed for field use for fast and accurate measurements of moisture in soil material. This is a true TDR instrument with automatic beginning and end point determinations and full graphing abilities, allowing determination of both time and impedance differences along a waveguide. The measuring range is 0-100% volumetric moisture content. The accuracy is +/– 2% FS or higher.

The in-situ temperature and moisture data were collected using temperature sensors buried in the subgrade during the reconstruction at section K2020 + 200 of the QTH. The sensor distribution map is shown in Fig. 6(a). The top width of the subgrade is 10 m, the height is 2 m, and the slope ratio is 1:1.5, extends 5 m to the right. The sensors are buried only in the right half subgrade, which is symmetric to the left. There are together 9 columns and 182 sensors in the right side of the subgrade.

Data was acquired twice per day at 6 AM and 2 PM. The mean value was used to represent the daily temperature. The isotherm map with the depth and time at the middle of the subgrade is shown in Fig. 6(b). The temperature varies more rapidly at test locations nearer to the ground. The temperature at the test site 0.5

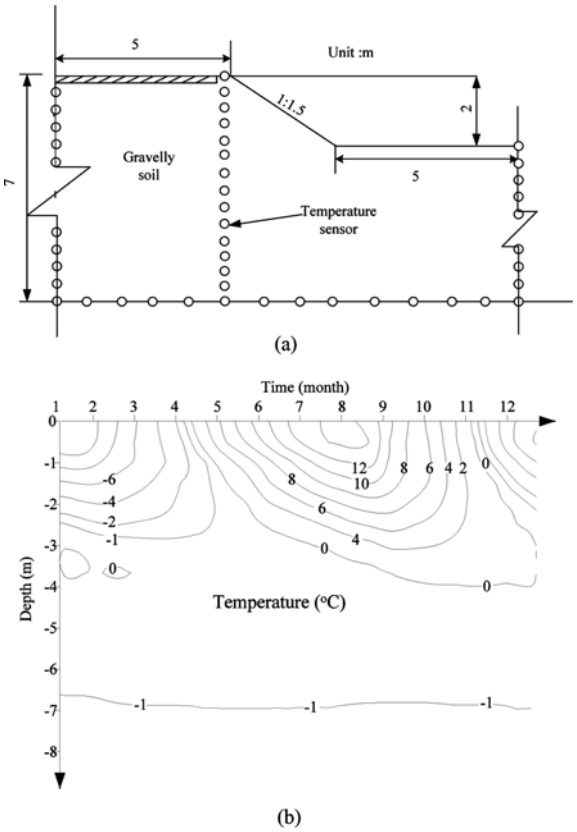

Fig. 6. *In-situ* Observation: (a) Single Field Model not Concerning the Moisture Movement, (b) Coupling Fields Model Concerning Moisture Movement

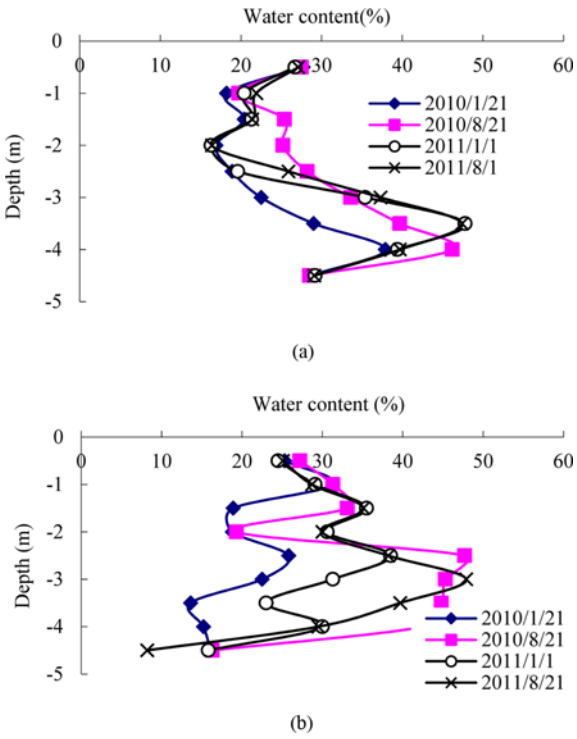

Fig. 7. Moisture Content with the Depth of the Subgrade: (a) Observation at the Middle, (b) Observation at the Shoulder

m under the ground reached its minimum in January and its maximum in July. The temperature of this test site increased from January to July and then decreased after July. After November, all the temperature was below 0°C in the -4 m depth, which means the soil became the permafrost below -4 m.

The moisture acquisition results at the middle and the shoulder of the subgrade are shown in Fig. 7. The pavement is asphalt. It can prevent the rain and snow from infiltrating into the subgrade. Under the ground the moisture content range from 20% to 50% above -5 m. It is 0°C below -5 m, which means the moisture has become the ice phase. There is no liquid water in the soil.

3. Mathematical Control Equation

The freeze and thaw cycles of permafrost subgrade are governed by the processes of heat and mass transfer accompanying heat flow and redistribution. Therefore, the equation describing the internal water and heat fields of the permafrost subgrade can be considered to be a heat transfer equation that considers moisture transport and phase changes (Wang and Hu, 2001; Li *et al.*, 2001; An, 1989; Sun *et al*., 2005; Zhang *et al.*, 2006).

3.1 Control Equation of the Temperature Field without Heat Exchange through Moisture Convection

$$\rho c\frac{\partial T}{\partial t}=\frac{\partial}{\partial x}\left(\lambda\frac{\partial T}{\partial x}\right)+\frac{\partial}{\partial y}\left(\lambda\frac{\partial T}{\partial y}\right)+Q+\rho L\frac{\partial f}{\partial t} \quad (1)$$

where, T is the instantaneous temperature (°C); t is the process period (s); λ is the coefficient of thermal conductivity (W/(m·°C)); ρ is the density of the soil (kg/m^3); c is the specific heat capacity of the soil (J/(kg·°C)); Q is the strength of the heat source (W/m^3); f is the volume of the solid water (ice content), also called the solid phase rate; L is the latent heat of the freezing and thawing phase change (J/kg); and x and y are the coordinates, x is the horizontal plane, y is depth into subgrade.

3.2 Control Equation of the Temperature Field Concerning the Heat Exchange of the Moisture Convection

The control Eq. (1) for the temperature field of the permafrost is based on variations in the thermal physics parameters of the soil and phase changes occurring in the soil. The parameter changes are induced by moisture migration, and the phase changes are driven by the temperature (Zhang *et al.*, 2006). Heat exchange through moisture convection is not included in Eq. (1). The solution for the temperature field coupled with this heat exchange is more complicated and is shown in Eq. (2):

$$\rho c\frac{\partial T}{\partial t}=\frac{\partial}{\partial x}\left(\lambda\frac{\partial T}{\partial x}\right)+\frac{\partial}{\partial y}\left(\lambda\frac{\partial T}{\partial y}\right)+Q+\rho L\frac{\partial f}{\partial t}+\rho_w c_w\frac{\partial(q_x T)}{\partial x}+\rho_w c_w\frac{(\partial q_y T)}{\partial y}$$

$$q_x=-D(\theta)\frac{\partial\theta}{\partial x}$$

$$q_y=-D(\theta)\frac{\partial\theta}{\partial y}-K(\theta) \quad (2)$$

where, ρ_w is the water density (kg/m^3); c_w is the specific heat capacity of the water (J/(kg·°C)); q_x is the water flux in the X direction (m/s); q_y is the water flux in the Y direction (m/s); θ is the volumetric water content (%); $D(\theta)$ is the expansion coefficient of the moisture contained in the soil; and $K(\theta)$ is the hydraulic conductivity of the soil.

3.3 Control Equation of the Moisture Field of the Permafrost Subgrade

The equation governing the transport of the soil moisture can be found by combining the fluid consistency equation and Darcy's Law and is shown in Eq. (3). The fluid consistency equation arises from applying the Quality Conservation Theorem to a fluid in a porous media (Ma *et al*., 2006; Cheng *et al*., 2008).

$$\frac{\partial\theta}{\partial t}=\frac{\partial}{\partial x}\left[D(\theta)\frac{\partial\theta}{\partial x}\right]+\frac{\partial}{\partial y}\left[D(\theta)\frac{\partial\theta}{\partial y}\right]+\frac{\partial}{\partial y}(K(\theta))-\frac{\rho_I}{\rho_w}\times\frac{\partial f}{\partial t} \quad (3)$$

where, ρ_I is the density of ice (kg/m^3), and the other variables are defined as in Eqs. (1) and (2).

4. Numerical Analysis

To analyze the effect of heat exchange through moisture convection on the thermal stability of the subgrade, a comparative study of the moisture movement is conducted. Coupling Eqs. (2) and (3) allows moisture transport to be considered in the thermal model, while Eq. (1) does not consider moisture movement.

The cross-section of the subgrade is depicted in Fig. 8(a). The top width of the subgrade is 10 m, the height is 2 m, and the slope ratio is 1:1.5, which are same to the dimensions of in-situ test subgrade. The subgrade is filled with gravelly soil. In Fig. 8(a), TB (Temperature Boundary) and MB (Moisture Boundary) represent the temperature and moisture boundary of the subgrade, respectively. 1, 2, 3, 4 and 5 represent the pavement, the left and right slope, the natural ground, the vertical limitation and the underground boundary location, respectively.

4.1 Grid Division of the Subgrade

4.1.1 Division in Space Domain

A commercially available finite element package (Ansys) is used to solve the simulation. The computational mesh used in the simulations is divided as shown in Fig. 8(b). The mesh is divided into triangular and quadrilateral units to ensure the accuracy of the calculation and efficient computation. There are 168,045 elements and 29,147 nodes in the moisture-temperature analysis mesh. The origin of the calculation region is the center of the subgrade, and the mesh extends 5 m to the left and right and 5 m in depth.

4.1.2 Division in Time Domain

The time period is defined to be 10 days such that there are 36 periods in a year. The calculation ends when the temperature has

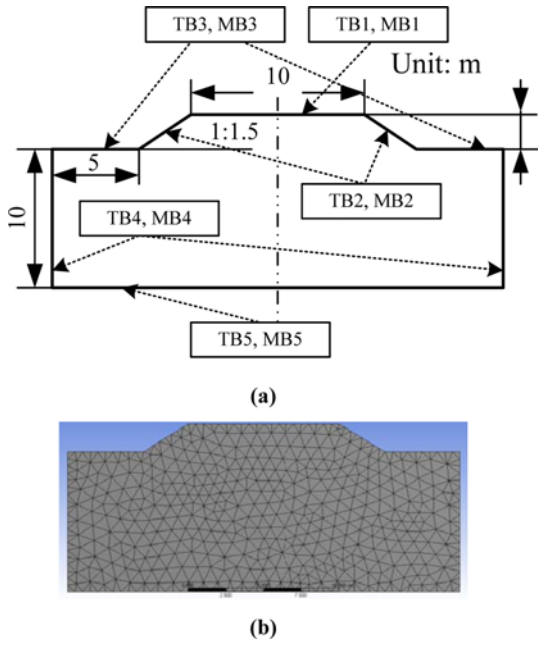

Fig. 8. Dimensional Size and Mesh Grid of the Subgrade: (a) Boundary Situation, (b) Computational Mesh

reached equilibrium with a tolerance of 0.01°C or the moisture with a tolerance of 0.1% (m^3/m^3).

4.2 Boundary Condition and Parameter Selection

4.2.1 Boundary Condition

The boundary condition of the temperature field is defined by the "Additional Surface Layer" principle, which is a physical layer with some pre-defined thickness attached to the lower underlying layer. The temperature and moisture fields are discontinuous across the boundary between the upper air layer and the bottom soil layer. The boundary is defined by fitting the in-situ test temperatures

The fitting function of the temperature boundary TB1, TB2 and TB3 are all sine functions, as shown in Eq. (4):

$$T = a + b\sin(ct + d) + 1.1 \times 10^{-4} t \tag{4}$$

where, T is the temperature in a particular day, t is the number of days since Jan. 1, and *a, b, c,* and *d* represent the parameters defined in Table 1.

The temperature boundary of the left and right vertical limitation TB4 is shown in Eq. (5):

Table 1. The Boundary Situation Parameters

Fit coefficient / Boundary situation	a	b	c	d
Pavement	2.85	-11.79	$-0.98 \times 2\pi/365$	1.84
Slope	0.60	-10.80	$-0.99 \times 2\pi/365$	1.93
Ground	-1.66	6.75	$-0.97 \times 2\pi/365$	-2.02

$$\begin{cases} T = -0.18 \\ T = -0.1205h^2 + 2.22 \times 10^{-4} t^2 + 0.0105th - 0.8969h - 0.06146t \\ \quad + 1.8486 \qquad t \le 180 \\ T = 0.1826h^2 - 8.77 \times 10^{-5}(t-180)^2 + 0.084h + 0.02853(t-180) \\ \quad - 0.0054(t-180)h - 2.288 \qquad t \le 180 \end{cases} \tag{5}$$

The temperature boundary of the underground boundary location TB5 is shown in Eq. (6):

$$T = -0.18 \tag{6}$$

The moisture boundary of the left and right slope of the highway MB2 is shown in Eq. (7)

$$\begin{cases} \theta = -0.0005t^2 + 0.1775t - 9.7055 & 70 \le t \le 180 \\ \theta = -0.0007(t-180)^2 + 0.038(t-180) + 7.4299 & 180 \le t < 320 \\ \theta = 0 & t \in others \end{cases} \tag{7}$$

The moisture boundary of The natural ground MB3 is shown in Eq. (8):

$$\begin{cases} \theta = -0.0005t^2 + 0.1688t - 9.087 & 70 \le t \le 180 \\ \theta = -0.0008t^2 + 0.0455t + 7.6471 & 180 \le t < 320 \\ \theta = 0 & t \in others \end{cases} \tag{8}$$

The moisture boundaries of MB1, MB4, and MB5 are shown in Eq. (9):

$$\theta = 0 \tag{9}$$

From November of the first year to March of the second year, the subgrade is frosted all in depth. So the water content is zero.

4.2.2 Selection of the Thermal Physics Parameters

The soil is tested in indoor experiments, and the soil belongs to GW. The heat conductivity coefficient λ_f and λ_u of the filling soil and the specific heat capacity C_f and C_u are shown in Eq. (10), which can be determined using a regression of the experimental data (Wu *et al.,* 2005):

$$\begin{aligned} \lambda_f &= 0.104 \times 10^{-3} r^{0.921} + 3.72 \times 10^{-5} r\theta; \\ \lambda_u &= 0.408 \times 10^{-3} r^{0.945} + 1.72 \times 10^{-5} r\theta; \\ C_f &= r(0.914 + 0.023\theta); \\ C_u &= r(0.865 + 0.041\theta) \end{aligned} \tag{10}$$

where, r is the dry density (kg/m^3), the subscript *f* denotes the freeze soil, and the subscript *u* denotes the unfrozen soil.

4.2.3 Selection of the Moisture Transport Parameters

The moisture conductivity ratio and the expansion coefficient are shown in Eq. (11):

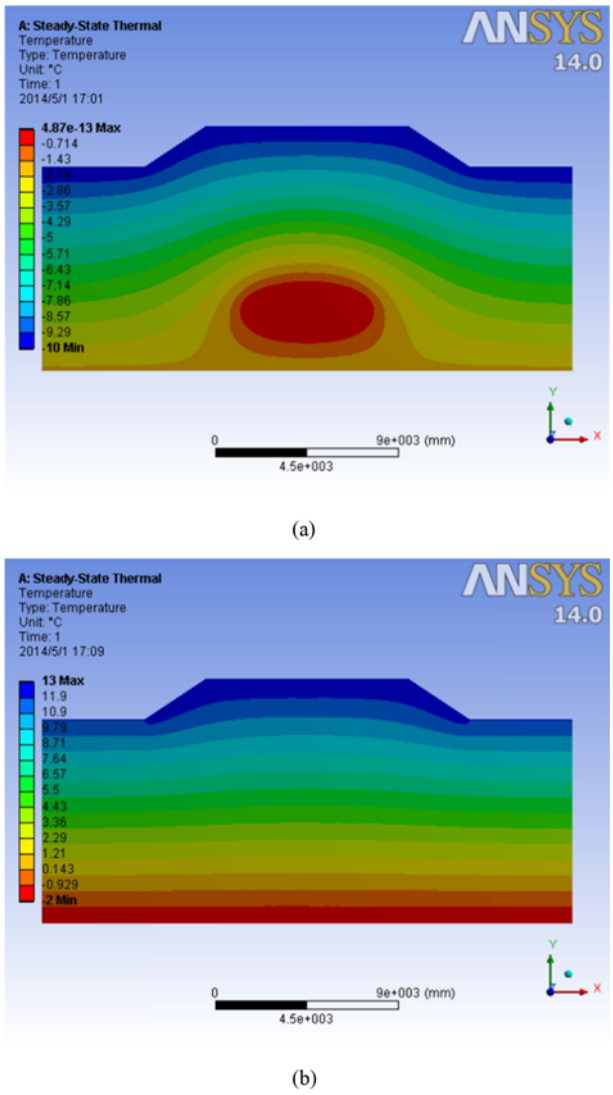

Fig. 9. Simulation Results by FEM: (a) Temperature in January, (b) Temperature in August

$$K_u = 2.9657^{-3}\,\theta^{11.2593}; \qquad K_f(\theta) = K(\theta)/I$$
$$D_u = 0.0064\times 10^{-3} e^{10.912\theta}; \qquad D_f(\theta) = D(\theta)/I \tag{11}$$

where, I is an experimental constant that can be approximated by the function $10^{10\theta_i}$, θ_I is the ice content of the soil, and the other parameters are defined as in the previous equations.

The simulation results are showed in Fig. 9. Figs. 9(a) and 9(b) show the temperature distribution in January and August, respectively. The freeze depth is -2 m in January and -5 m in August. There is some permafrost region in QTH all the year.

5. Discussions

5.1 Numerical Calculation

The calculated temperatures vs. depth in the subgrade are redrawn, as shown in Fig. 10. The calculated temperatures using

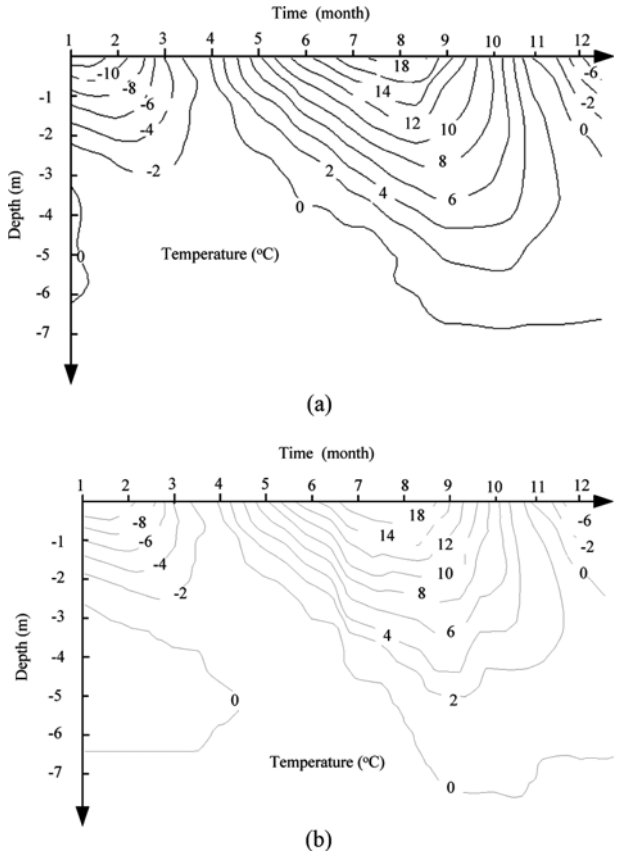

Fig. 10. Temperature Distribution of the Subgrade: (a) Single Field Model not Concerning on the Moisture Movement, (b) Coupled Fields Model Concerning the Moisture Movement

models including and omitting moisture transport are presented in Figs. 10(a) and 10(b), respectively. These images lead to three conclusions. 1) When moisture transport is considered, the descending trend observed in the upper boundary of the freeze region within the subgrade is enhanced, and the seasonal thaw depth of the subgrade is deepened. The maximum freeze depth is 6.8 m in October if moisture transport is disregarded. However, this depth is 7.4 m, which is 0.6 m deeper, when moisture movement is considered. The maximum thaw depth equals the depth of the 0°C contour of the temperature field. 2) The life cycle of the unfrozen soil core in the subgrade is increased when moisture movement is considered. In Fig. 10(a), the entire subgrade is frozen by the middle of January. However, when heat exchange through moisture transport is considered, the entire subgrade is not frozen until the end of April, as shown in Fig. 10(b). 3) All the soil became into permafrost near -6.8 m depth in Fig. 10(a), however the depth deepened to -7.1 m in Fig. 10(b).

5.2 Comparison Analysis

Figures 11(a) and 11(b) present the calculated and observed temperatures vs. depth at the middle of the subgrade at Section K3020 + 200 on Jan. 20th and August 20th respectively. The calculated values are generally in agreement with the observed

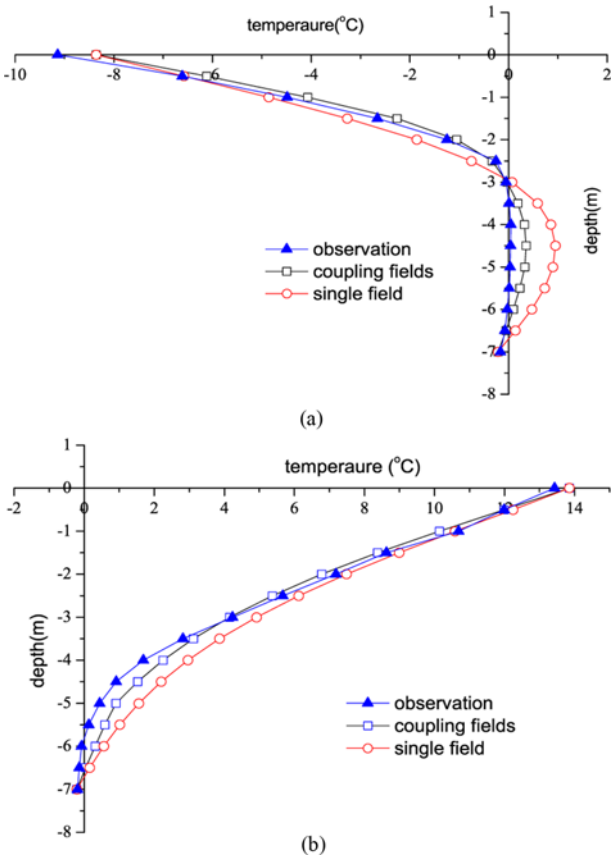

Fig. 11. Numerical and Infield Data Compare: (a) Subgrade Cross Section in January, (b) Subgrade Cross Section in August

values. The strongest agreement between the two fields is achieved 3 m beneath the subgrade surface. However, in the region near the phase change boundary, the difference between the calculated and observed values is large. The largest errors produced using the single-field model are 1.28 and 0.91 in January and August, respectively. However, the maximum errors decreased to 0.61 and 0.32 using the coupled-fields model. Therefore, it can be concluded that the temperature distribution is affected by the moisture content of the soil. The thermal characteristics of the soil, particularly the specific heat and thermal conductivity, vary with the moisture content of the soil.

The model simulations were compared with field data collected in January and August at Section K3020 + 200. The simulated soil temperatures were in strong agreement with the measured data. The simulation results of the coupled-fields model agree with the data more strongly than those of the single field model. The coefficients of correlation for the coupled-field model *are* 0.997 and 0.998 in August and January, respectively, while those for the single-field model are 0.996 and 0.982 in August and January, respectively. The coupling model is an enhanced tool for highway design that predicts the soil moisture field as a function of depth and assesses the availability of soil moisture. This model can aid in prevention of highway damage by predicting periods of subgrade thaw and elevated water content such that traffic restrictions can be effectively implemented.

6. Conclusions

A finite element method was used to develop a 2-D model of the highway subgrade. Numerical calculations were performed to obtain the non-uniform temperature distribution in the subgrade. The model predictions were compared with the in-situ test results and appeared to be in strong agreement. The simulation results of the coupled-fields model agree with the data more strongly than those of the single-field model. The coefficients of correlation for the coupled-field model are 0.997 and 0.998 in August and January, respectively, while those for the single-field model are 0.996 and 0.982 in August and January, respectively. The coupled-fields model can improve the prediction precision of temperature distribution and further to predict the qualitative and quantitative behaviors of the subgrade. Therefore, the coupled model is superior to the traditional single-field model in both accuracy and precision and can provide a valuable tool for highway construction and the prevention of highway damage by predicting periods of subgrade thaw and elevated water content such that traffic restrictions can be effectively implemented.

Acknowledgements

The authors gratefully acknowledge support from the State Natural Sciences Fund of China (No. 50701044 and No. 51378072).

References

An, W. (1989). *Interaction among temperature moisture and stress fields in frozen soil*, Lanzhou University Press, Lanzhou, pp.183-211 (in Chinese).

Chen, D., Qian, C., Miao, C., and Liu, J. (2010). "Hybrid analytic-FEM approach for calculating coupling hygro-thermal deformation of concrete." *Journal of Southeast University (Natural Science Edition)*, Vol. 40, No. 1, pp. 89-95 (in Chinese).

Cheng, G. D., Sun, Z. Z., and Niu, F. J. (2008). "Application of the roadbed cooling approach in qinghai-tibet railway engineering." *Cold Regions Science and Technology*, Vol. 52, No. 1, pp. 1-25, DOI: 10.1016/j.coldregions.2007.02. 006.

Fortino, S., Genoese, A., Genoese, A., and Rautkari, L. (2013). "FEM simulation of the hygro-thermal behaviour of wood under surface densification at high temperature." *Journal of Materials Science,* Vol. 48, No. 1, pp. 7603-7612, DOI: 10.1007/s10853-013-7577-1.

Gatmiri, B., Maghoul, P., and Duhamel, D. (2010). "Two-dimensional transient thermo- hydro- mechanical fundamental solutions of multiphase porous media in frequency and time domains." *International Journal of Solids and Structures*, Vol. 47, No. 5, pp. 595-610, DOI: 10.1016/j.ijsolstr. 2009.10.022.

Harlan, R. L. (1973). "Analysis of coupled heat-fluid transport in partially frozen soil." *Water Resources Research*, Vol. 9, No. 5, pp. 1314-1323.

Harlan, R. L. and Nixon, J. F. (1979). "Ground thermal regime." *Geotech. Eng. for Cold Regions*, Vol. 12, No. 3, pp. 103-150.

Klimenta, D., Radosavljevic, J., and Jevtic, M. (2011). "An improved non-adiabatic FEM model of a line-to-earth fault in buried power cables." *International Journal of Heat and Mass Transfer*, Vol. 54,

No. 6, pp. 3514-3522, DOI: 10.1016/ j.ijheatmasstransfer. 2011.03.034.

Li, H., Liu, Z., and Liang, C. (2001). "Mathematical model for coupled moisture, heat and stress field and numerical simulation on frozen soil." *Acta Mechanica Sinica*, Vol. 33, No. 8, pp. 621-627.

Ma, W., Shi, C. H., and Wu, Q. B. (2006). "Monitoring study on technology of the cooling roadbed in permafrost region of qinghai-tibet plateau." *Cold Regions Science and Technology*, Vol. 44, No. 1, pp. 1-11, DOI: 10.1016/j.coldregions.2005.06.002.

Mao, X., Hu, C., and Hou, Z. (2004). "Laboratory large-scale test of temperature field in permafrost sub-grade." *Journal of Chang'an University (Natural Science Edition)*, Vol. 24, No. 1, pp. 30-34 (in Chinese).

Miller, R. D. (1972). *Freezing and heaving of saturated and unsaturated soils,* Highway Research Report, No. 393, pp. 1-11.

Sun, B. X., Xu, X. Z., and Lai, Y. M. (2005). "Evaluation of fractured rock layer heights in ballast railway embankment based on cooling effect of natural convection in cold regions." *Cold Regions Science and Technology*, Vol. 42, No. 2, pp. 120-144, DOI: 10.1016/ j.coldregions.2005.01.001.

Tekeste, M. Z., Tollner, E. W., and Raper, R. L. (2009). "Non-linear finite element analysis of cone penetration in layered sandy loam soil - Considering precompression stress state." *Journal of Terramechanics*, Vol. 46, No. 5, pp. 229-239, DOI: 10.1016/ j.jterra.2009.05.005.

Tekeste, M. Z., Raper, R., L., Tollner, E. W. (2007). "Finite element analysis of cone penetration in soil for prediction of hardpan location." *Transactions of the ASABE*, Vol. 50, No. 1, pp. 23-31, DOI: 10.1155/2012/548620.

Trcala, M. (2012). "A 3D transient nonlinear modelling of coupled heat, mass and deformation fields in anisotropic material." *International Journal of Heat and Mass Transfer*, Vol. 55, No. 12, pp. 4588-4596, DOI: 10.1016/j.ijheatmasstransfer.2012.04.009.

Wang, T. and Hu, C. (2001). "A numerical model of moisture migration for frozen soil subgrade." *China Journal of Highway and Transport*, Vol. 14, No. 4, pp. 5-8, DOI: 10.3321/j.issn:1001-7372.2001.04.002.

Wang, S. Y., Chan, D. H., and Lam, K. C. (2010). "Numerical and experimental studies of pressure-controlled cavity expansion in completely decomposed granite soils of Hong Kong." *Computers and Geotechnics*, Vol. 37, Nos. 7-8, pp. 977-990, DOI: 10.1016/ j.compgeo.2010.08.006.

Wu, J. M., Wang, S. J., and Zhang, J. Z. (2005). *The highway engineering on permafrost regions*, China Communication Press, Beijing.

Xia, K. (2011). "Finite element modeling of tire/terrain interaction: Application to predicting soil compaction and tire mobility." *Journal of Terramechanics*, Vol. 48, No. 2, pp. 113-123, DOI: 10.1016/ j.jterra.2010.05.001.

Xu, X., Wang, J., and Zhang, L. (2001). *Frost physics[M],* Science Publish House, Beijing.

Zhang, M. Y., Lai, Y. M., and Niu, F. J. (2006). "A numerical model of the coupled heat transfer for ductventilated embankment under wind action in cold regions and its application." *Cold Regions Science and Technology*, Vol. 45, No. 2, pp. 103-113, DOI: 10.1016/ j.coldregions. 2006.03.002.